Dedicated to Prof. Ioan-Iovitz Popescu's 75th Anniversary

THE CHANNEL-SPARK DISCHARGE AS A PULSED, INTENSE ELECTRON AND X-RAY SOURCE

M. NISTOR, N. B. MANDACHE

National Institute for Lasers, Plasma and Radiation Physics, Plasma Physics and Nuclear Fusion Laboratory (Lab. 22), P.O. Box. MG-36, 76900 Bucharest-Magurele, Romania
E-mail: mnistor@infim.ro

Abstract. This work is focused on the characteristics of the pulsed electron beam produced in a channel-spark discharge. The beam measurements were made using the self-biasing method of a Faraday cup. We studied also the X-ray emission produced at the electron beam interaction with a target. The dependence of the beam current and energy and of the X-ray intensity on working gas pressure and external capacitor value has been investigated. The pulsed electron beam is polyenergetic and the mean energy of electrons is decreasing in time during the pulse. The information concerning the electron beam characteristics is directly related to an efficient ablation of targets and thus to the growth of high quality thin films. The X-ray emission characteristics prove the feasibility of a compact, pulsed X-ray source, of low energy photons (less than about 10 keV), based on the channel-spark discharge.

Key words: channel-spark, pulsed electron beam, X-ray emission.

1. INTRODUCTION

The discovery of the pseudospark discharge in 1979 by J. Christiansen and C. Schultheiss [1] has opened up the way for a lot of studies on pulsed electron beams and applications in material processing, thin film deposition, lithography, compact X-ray sources, etc.

Pulsed, intense electron beams are produced in transient hollow cathode glow discharges, at gas pressure in the range 10^{-3}–10^{-1} mbar and applied voltages of few kV up to tens of kV. The break-down voltage of these abnormal discharges is on the left hand branch of the Paschen curve. Typical examples are the pseudospark discharge [1], the channel-spark discharge [2], and the preionized controlled open-ended hollow cathode discharge (PCOHC) [3, 4]. These discharges differ one from another mainly by the geometry, working gas pressure and beam characteristics [5]. The parameters of the pulsed electron beams produced in such discharges are: currents of tens–hundreds of A, pulse widths of tens–hundreds of ns, and energies up to the value eU where U is the applied voltage.

After the apparition of the pseudospark few studies were dedicated to the deposition of thin films of high temperature superconductors ($YBa_2Cu_3O_{7-x}$) by using pulsed electron beams for target ablation [6–9], in order to find a cheaper alternative to pulsed laser deposition. The propagation of a collimated intense pulsed electron beam in gas over few centimetres from the anode to the target is affected by space charge effects, even if partial space charge neutralization takes place by ionizations processes produced in the working gas. The channel-spark discharge was successfully used to grow thin films due to its specific feature, the presence of a capillary tube in which the electron beam is produced and guided to the target. These results opened the way of the method called Pulsed Electron beam Deposition (PED).

Compared to lasers with similar power densities ($\sim 10^8$ W/cm^2), potential advantages of pulsed electron beam sources include higher electrical efficiency than lasers, the ability to process materials that are transparent or highly reflective to laser light and lower capital costs [10]. On the other hand, the pressure domain in which takes place the growth of thin films is restricted compared to laser ablation, due to the narrow working pressure range of the high voltage abnormal discharge.

Only few studies were focused on the characteristics of the pulsed electron beam produced in the channel-spark discharge compared to pseudospark and PCOHC discharges, which were intensively studied.

The investigations reported here are focused on measurements of the electron beam parameters by a self-biasing method and by X-ray emission recorded at the electron beam interaction with a target. The dependence of the beam current and energy and of the X-ray intensity on working gas pressure and external capacitor value has been investigated. The information concerning the electron beam characteristics is directly related to an efficient ablation of targets and thus to the growth of high quality thin films.

2. EXPERIMENTAL SET-UP

The pulsed electron beam source based on channel-spark discharge geometry consists of a hollow cathode, a capillary tube and a grounded anode, which is the experimental chamber (Fig. 1a). The electron beam is guided towards the target by a quartz capillary tube, which has 5 mm diameter and 100 mm length. The working gas was argon at a pressure in the range $10^{-2} - 4 \times 10^{-2}$ mbar.

In our experiments the external capacity, mounted between the hollow cathode and the grounded anode, was varied between 2 and 16 nF, and the applied voltage between 14 and 17 kV. The repetition rate was about 1 Hz. The parameter pd, where p is the working gas pressure and d is, in this configuration, the diameter of the capillary tube, corresponds to the left hand branch of the Paschen curve.
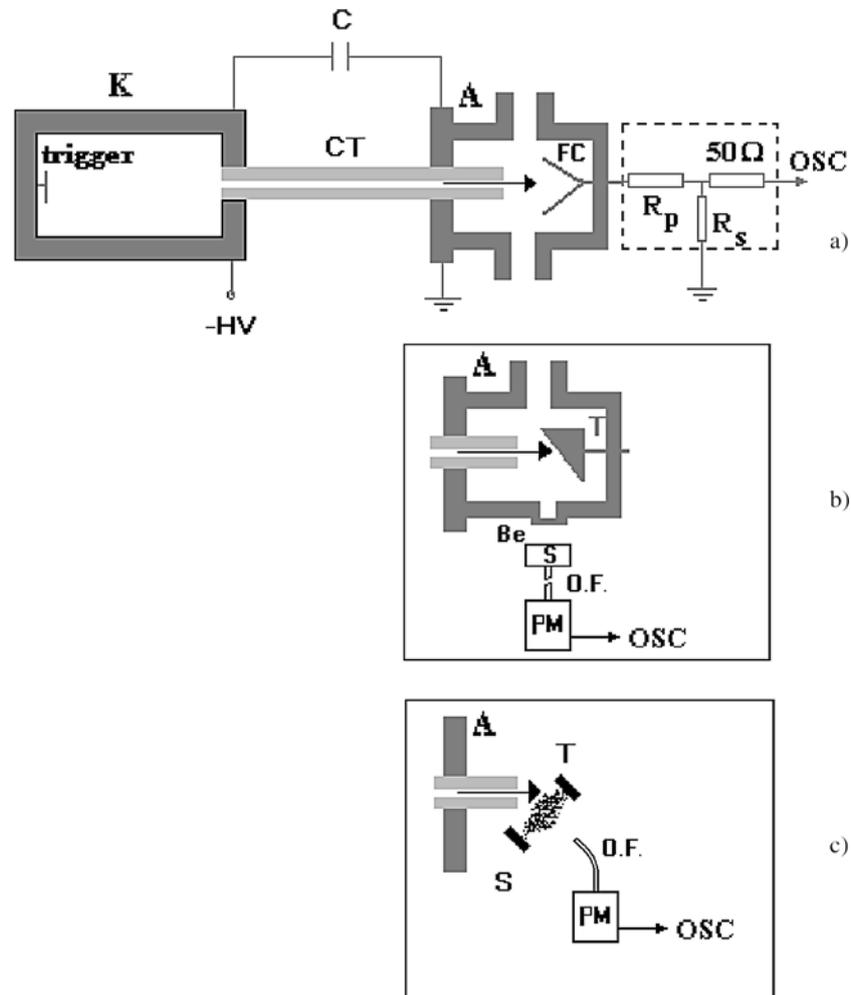
Fig. 1 a) Experimental set-up of the channel-spark discharge: K – hollow cathode, CT – capillary tube, A – anode, C – capacitor, FC – Faraday cup, OSC – oscilloscope; b) X – ray measurements set-up, S – scintillator, OF – optical fiber, PM – photomultiplier; c) ablation set-up, T – target, S – substrate.

The capacitor is charged initially to the high voltage and the break-down between the cathode and the anode is initiated by a pre-ionization plasma produced into the hollow cathode by a secondary low current discharge between the trigger electrode and the hollow cathode. The pulsed electron beam is produced during the break-down phase of the high voltage abnormal discharge.

The high voltage (U_d) on cathode was measured with a Tektronix P6015A voltage probe. The electron beam current was measured with a Faraday cup connected to ground by a shunt resistor $R_s = 0.3\ \Omega$. The Faraday cup was placed axially at 10 mm

from the anodic end of the capillary tube (Fig. 1a). The oscillograms were recorded using a 100 MHz bandwidth oscilloscope Tektronix TDS 320.

The energy characterization of the electron beam was made using the method described in reference [11]. The Faraday cup is self-biased with respect to ground to a negative potential $V_p = R_P \times I_b$, where R_p is a resistor ($R_P >> R_s$) connected in series with the shunt (Fig. 1a) and I_b is the collected electron beam current. The slow electrons are repelled and only electrons with energies higher than the value eV_p are collected by the Faraday cup. Varying the values of the resistor R_P different self-biasing voltages were obtained.

The X-ray emission produced at the interaction of the electron beam with a target placed at an angle of 45° to the axis was recorded using a NE102A plastic scintillator coupled to a fast photomultiplier by an optical fiber (Fig. 1b). The scintillator was covered with a 6 μm Al foil to prevent ambient light to enter to the photomultiplier. The X-ray radiation passes through a beryllium window of 15 μm before leaving the experimental chamber.

For optimum parameters of the beam an ablation plasma is produced at the interaction of the electron beam with a target, leading to the growth of thin films on a substrate (S) placed parallel with the target, at 3–4 cm distance (Fig. 1c). The luminosity of the ablation plasma was recorded using an optical fiber coupled to a photomultiplier.

3. EXPERIMENTAL RESULTS AND DISCUSSIONS

3.1. SELF-BIASING MEASUREMENTS

Fig. 2 shows typical oscillograms of the discharge voltage (top trace), electron beam current (middle trace) and luminous signal of the ablation plasma produced at the interaction of the electron beam with a hydroxyapatite target (bottom trace), recorded in two separate experimental configurations (Fig. 1a and Fig. 1c respectively). The current was measured with the Faraday cup connected to the $R_s = 0.3 \ \Omega$ shunt.

The electron beam current (middle trace in Fig. 2) increases simultaneously with the discharge voltage fall and reaches a maximum of about 800 A when the discharge voltage has decreased to a few kV. The electron beam current has a pulse width (FWHM) of 150 ns. The discharge voltage falls to zero in approximately 200 ns.

After this beam phase of the discharge, which lasts about 200 ns, when the current is carried by electrons with energies from a few keV to a maximum value equal to eU_d, there is a low voltage discharge phase with damped oscillations (top trace in Fig. 2) lasting many hundreds of ns, when the current is carried by low energy (thermal) electrons.
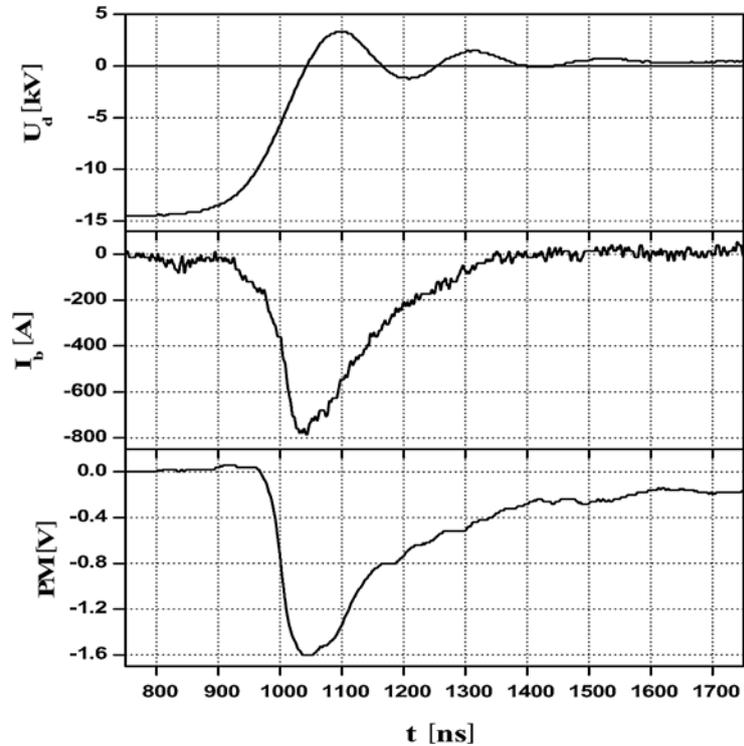
Fig. 2 – Temporal evolution of the discharge voltage (top), the electron beam
current (middle) and the total luminous signal of the ablation plasma (bottom).

Since the ablation plasma is produced at the interaction of the electron beam
with the target, the begining of the luminous emission is correlated with the
electron beam current rise. From the bottom trace in Fig. 2 we noticed that the
ablation plasma lasts a few microseconds. This is in accord with our spectroscopic
measurements [12] where the presence of single ionized ions were recorded up to
few microseconds after the beam phase.

Measurements of the discharge voltage, beam current and X-ray emission
were performed in the whole working gas pressure range ($10^{-2} - 4 \times 10^{-2}$ mbar).

In Fig. 3 are shown the discharge voltage (U_d), electron beam current (I_b) and
self-biasing potential (V_p) for $R_p = 50\ \Omega$. The applied voltage was 16 kV and the
working gas pressure was about 10^{-2} mbar. This is the lowest pressure at which the
cathode-anode breakdown takes place in our channel-spark discharge
configuration. The self-biasing potential was measured with the high voltage probe
mounted at the exit of the Faraday cup.

The maximum beam current has about 160 A and the pulse duration (FWHM)
is rather large, about 170 ns. The maximum value of the self-biasing potential is
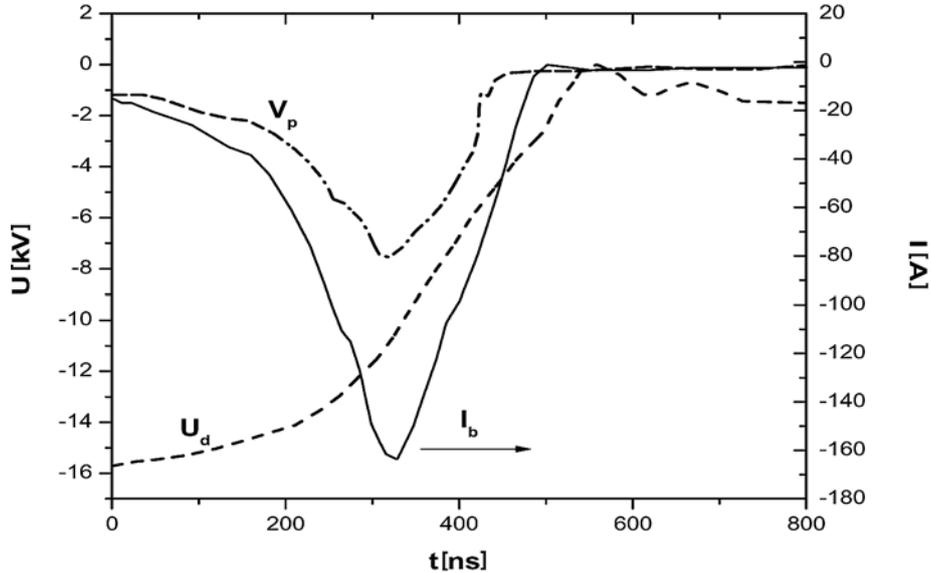7.5 kV, less than the value of the discharge voltage at that moment with about 4 kV.

Fig. 3 – Discharge voltage (U_d), electron beam current (I_b) and self-biasing potential (V_p) for
$R_p = 50\ \Omega$, at low pressure.

Hence, in this low pressure regime of the channel-spark discharge a maximum current of 160 A of electrons with energies higher than 7.5 keV was evidenced.

In the high pressure regime (4×10^{-2} mbar) the voltage fall and in consequence the electron beam pulse last less than in the low pressure regime. In such a high pressure regime we recorded the highest self-biasing potential (Fig. 4).

A maximum current of approximately 200 A of electrons with energies higher than 9 keV was recorded, but the FWHM is only 50 ns.

Since the total beam current measured without self-biasing ($R_p = 0$) is about 800 A (Fig. 2) it results that in both low and high pressure regime the majority of electrons in the beam have low and medium energies, less than about 7.5 keV, respectively 9 keV. The electron energy distribution is a polyenergetic one, with higher energy electrons at the beginning of the voltage fall, and a dominant component of medium and low energy electrons increasing in time, during the voltage fall [11].

Most of the electrons in the beam are concentrated in a diameter smaller than 2 mm, as proved by the trace observed on the surface of the target after beam-target interaction. Based on these self-biasing measurements we estimated a fluence of the electron beam up to 5 J/cm^2.

The range of the electrons of the beam in the target gives the order of magnitude of the thickness of evaporated material. Having a polyenergetic energy distribution decreasing with energy increase, the electron beam gives an energy deposition profile into the target with a maximum near the target surface [2].
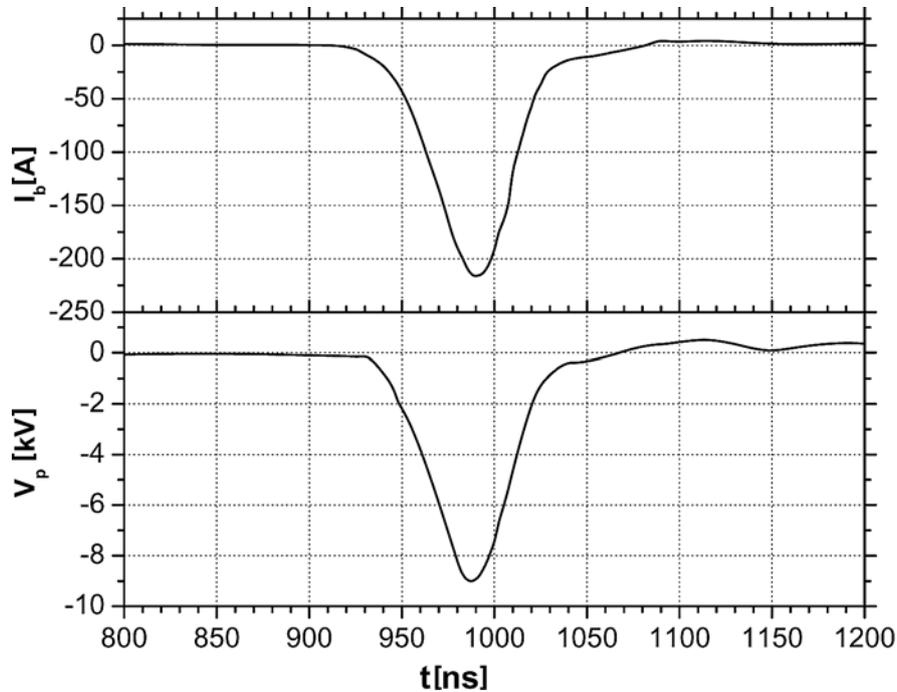
Fig. 4 – Electron beam current (top) and self-biased voltage (bottom) at high pressure.

Our ablation experiments [12] are in accordance with the work of Dewald [13] and Witke [14], which proved that the channel-spark working in the low-pressure regime is more efficient for ablation of targets and thin-film depositions.

3.2. X-RAY MEASUREMENTS

Since the thin-film deposition is efficient in the low pressure regime most of the X-ray measurements (see Fig. 1b) were made at a working pressure of about 10^{-2} mbar. The influence of the capacitor value on the X-ray signal was investigated.

In Fig. 5 are shown the discharge voltage and the X-ray signal, for an applied voltage of 17 kV and a capacitor value of 3 nF. The X-ray signal has a double structure, with the first peak simultaneous with the beginning of the discharge voltage fall.

The same signals but for a capacitor value of 6 nF are presented in Fig. 6. The intensity of the first X-ray peak is approximately the same with that presented in Fig. 5, but the second peak is about 4 times higher than the corresponding peak in Fig. 5.

The X-ray emission duration (FWHM) is about 70 ns, less than the FWHM of the beam current I_b (Fig. 3), since the X-ray photons produced by the low energy
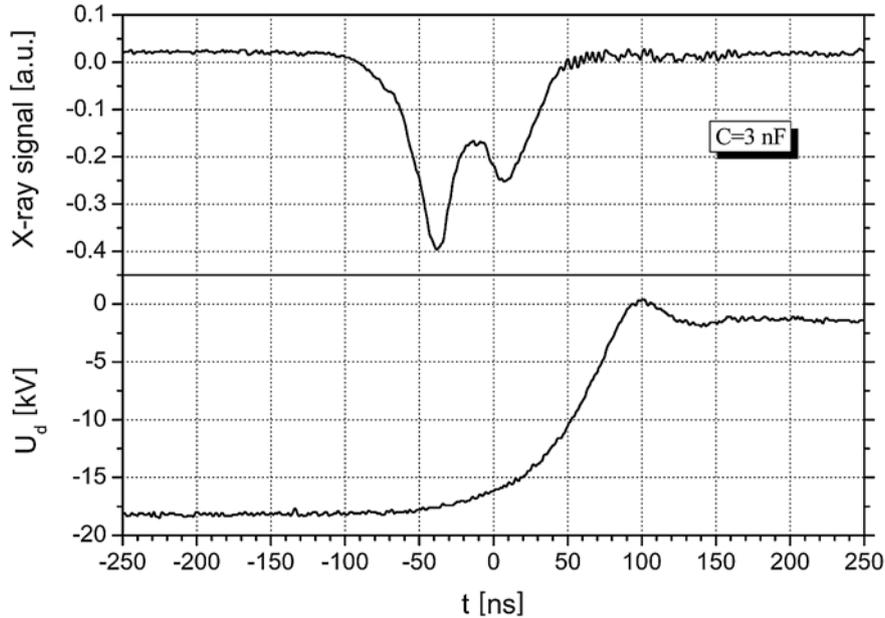
Fig. 5 – Oscillograms of the X-ray signal (top) and discharge voltage U_d (bottom) at low pressure for C = 3 nF.

electrons (less than about 2–3 keV) which are the main component of the beam at later times, are absorbed before arriving in the scintillator.

Since high energy electrons are produced at the beginning of the pulse and medium and low energy electrons towards later times [11], the increase of the second X-ray peak when the capacitor value was raised from 3 to 6 nF (Figs. 5 and 6) is due to the increase of the number of medium energy electrons in the beam. The high energy component of electrons remains constant, as proved by the first X-ray peak which remains practically constant.

These results are confirmed by the measurement presented in Fig. 7: the X-ray signals recorded with and without an Al foil of 25 μm in front of the scintillator. The first peak of the X-ray signal decreased 1.5 times and the second peak two times in the presence of the Al foil. This means that the first X-ray peak is due to electrons with energies higher than the energies of the electrons which produced the second X-ray peak.

In Fig. 8 are shown the discharge voltage and the X-ray signal for a capacitor value of 16 nF. On the same figure is given the filtered X-ray emission by Al foils having thickness of 20 μm and 60 μm. The double peak structure emerged into one X-ray pulse as compared with the above presented cases (C = 3 nF and 6 nF). The FWHM is practically the same, about 70 ns.

Adding Al foils in front of the X-ray detector the cut-off X-ray photon energy increases with foil thickness, leading to a selection in energy of the X-ray photons.
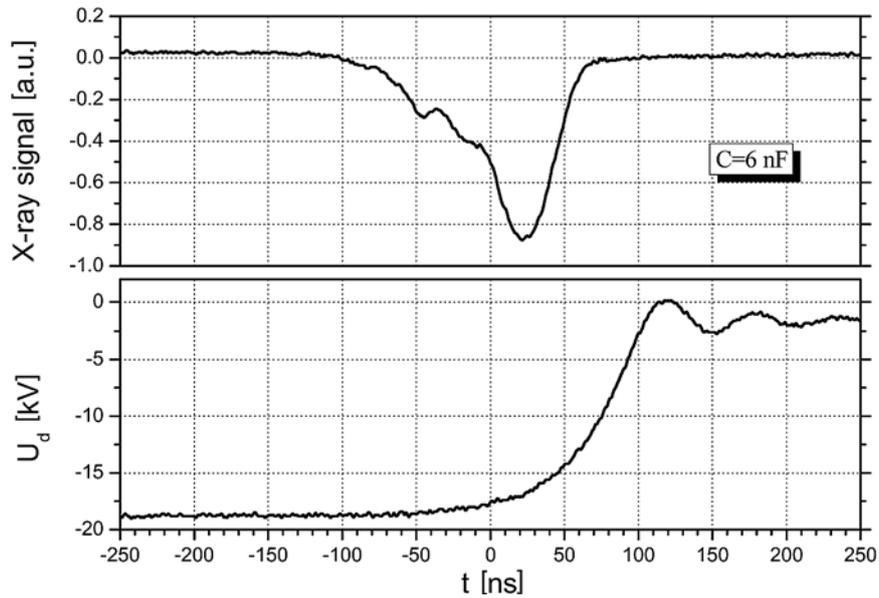
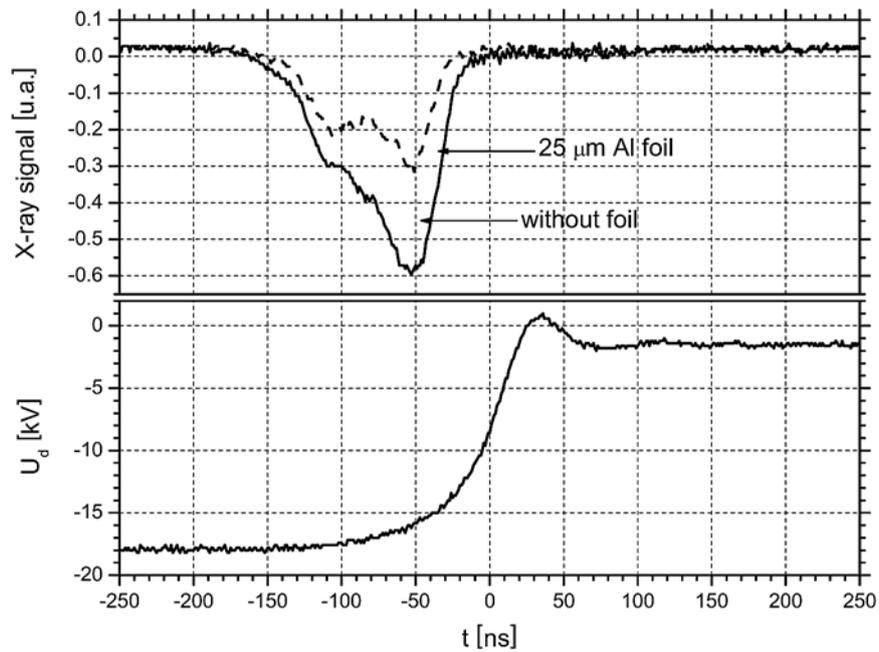Fig. 6 – Oscillograms of the X-ray signal (top) and discharge voltage U_d (bottom) at low pressure for $C = 6$ nF.

Fig. 7 – Oscillograms of the X-ray signals with and without Al foil (top) and discharge voltage U_d (bottom) at low pressure for $C = 6$ nF.
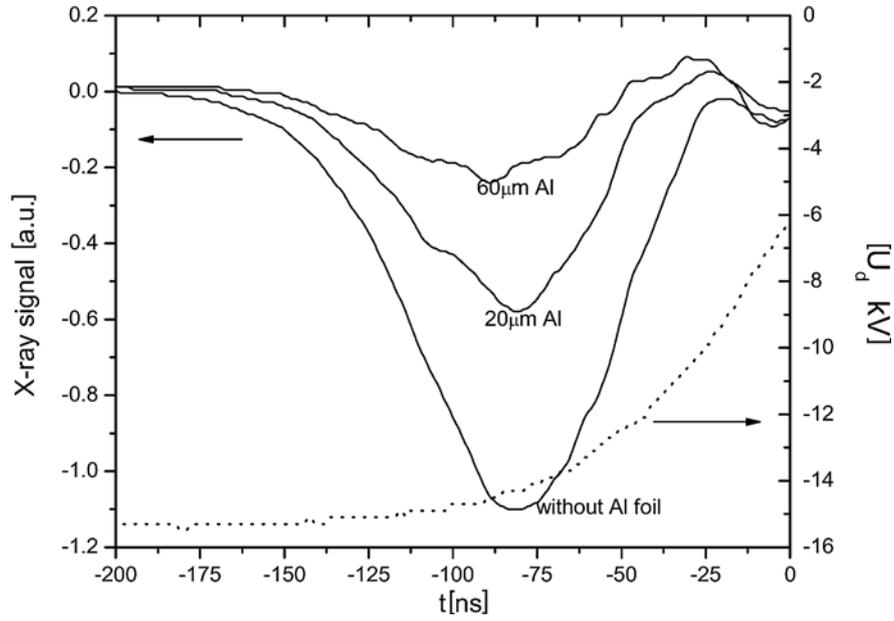
Fig. 8 – Discharge voltage and X-ray signals for 20 and 60 μm Al foil and without Al foil, at low pressure for C = 16 nF.
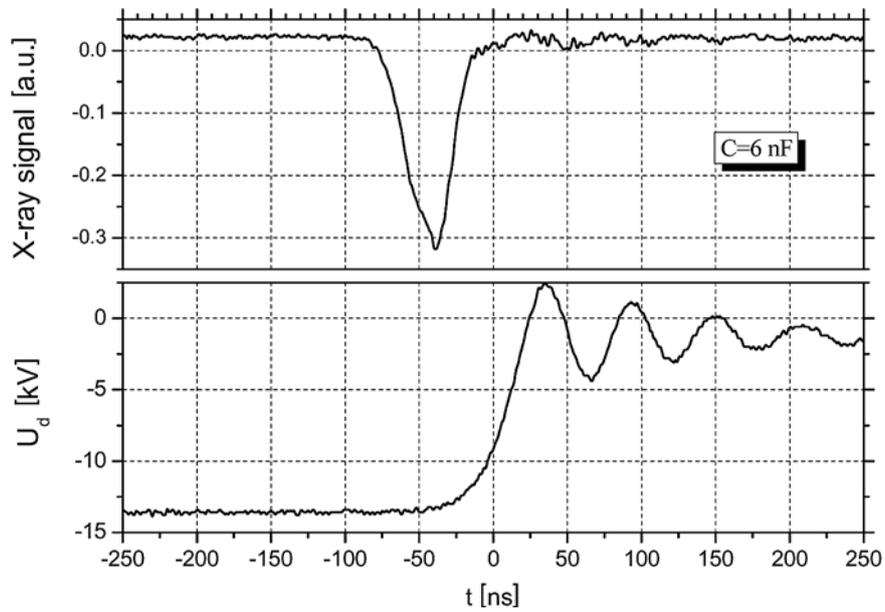

Fig. 9 – Oscillograms of the X-ray signal (top) and discharge voltage (U_d) (bottom) at high pressure for C = 6 nF.

The transmission of the 20 μm Al foil is 0.1 at about 4 keV photon energy, which means that at the X-ray signal recorded contribute photons with energies higher than about 4 keV, which are produced only by electrons with energies higher than 4 keV. The transmission of the 60 μm Al foil is 0.1 at about 6 keV photon energy, which means that the X-ray emission is due to electrons with energies higher than 6 keV.

The maximum of the X-ray emission filtered with the 60 μm Al foil is displaced towards earlier times in comparison with the maximum of the X-ray emission without Al foil which confirm the above results that higher energy electrons are produced at earlier times.

In Fig. 9 is given the X-ray emission in the high pressure regime $(4 \times 10^{-2}$ mbar) for $C = 6$ nF. There is no double structure like in the low pressure regime for the same value of C (see Fig. 6) and the FWHM is only 30 ns. The beam phase of the discharge is shorter as proved also by the duration of the break-down fall. It results that the electron beam duration is inverse proportional with the working pressure value.

4. CONCLUSIONS

Measurements of the electron beam parameters were made by a self-biasing method and by X-ray emission recorded at the electron beam interaction with a target. The dependence of the beam current and energy and of the X-ray intensity on working gas pressure and external capacitor value has been investigated.

The pulse duration of the electron beam produced in the channel-spark is higher than in the pseudospark and PCOHC discharge [5]. In the low pressure regime, which is the best for thin film deposition, the pulse duration is more than 100 ns.

The presence of a capillary tube in which the electron beam is produced and guided to the target to be ablated, avoids the problems related with the beam propagation on a few cm from the anode to the target, encountered in the case of pseudo-spark and PCOHC.

For small capacitor values the X-ray emission has a double structure with the second peak increasing for higher capacitor values. This means the component of medium energy electrons from the beam increases with capacitor value.

The pulsed electron beam is poly-energetic, the mean energy of electrons decreasing in time during the pulse. The energy deposition of this poly-energetic electron beam is near the target surface. This prevents a subsurface heating, which can produce droplets in the ablation process. Indeed in the low pressure regime films with low density of droplets were obtained [15]. At this could contribute also the low energy electrons from the beam, which are dominant towards the end of the pulse, which melt the droplets resulted in the ablation process.

Since the anode is the experimental chamber, the channel-spark discharge configuration determines a long lasting plasma in the chamber (about 1.7 μs), thus

the thin film deposition is plasma-assisted. As in the case of pulsed laser deposition, the ablation plasma mediates the thin film formation on the substrate surface with a stoichiometry identical with that of the target [15].

The good reproducibility of the X-ray signals from one pulse to the other demonstrates a good reproducibility of the energy characteristics of the electron beam, which is important for a constant rate of ablation.

The X-ray emission characteristics prove the feasibility of a compact, pulsed X-ray source, of low energy photons (less than about 10 keV), based on a channel-spark discharge.

REFERENCES

1. J. Christiansen, C. Schultheiss, Production of high current particle beams by low pressure spark discharges, *Z. Phys.* A, **290**, 35–41 (1979).
2. G. Müller, M. Konijnenberg, G. Kraft, C. Schultheiss, Deposition by means of pulsed electron beam ablation; in *Science and Technology of Thin Film*, World Scientific Publ. Co. PET. LTD, 1995.
3. M. Ganciu, G. Modreanu, A. M. Pointu, I. I. Popescu, Generation of intense pulsed electron beams by superposition of two discharges, *J. Phys. D: Appl. Phys.*, **27**, *1*, 1370–1374 (1994).
4. M. Nistor, P. Charles, M. Ganciu, M. Lamoureux, N. B. Mandache, A. M. Pointu, Electron Energy Distribution Function in a Transient Open-Ended Hollow Cathode Discharge *Plasma Sources Sci. Technol.*, **11**, 183–189 (2002).
5. E. Dewald, K. Frank, D. H. H. Hoffmann, A. Tauschwitz, Comparative studies on intense electron beams generated in transient hollow-cathode discharges, *IEEE Trans. Pl. Sci.*, **30**, *5*, 1820–1826 (2002).
6. H. P. Schlolch, P. Fickenscher, T. Redel, M. Stetter, G. Saemann-Ischenko et al., Production of $Yba_2Cu_3O_{7-x}$ superconducting thin films by pulsed pseudospark electron beam evaporation, *Appl. Phys. A*, **48**, 397–400 (1989).
7. W. Benker, J. Christiansen, K. Frank, W. Hartman, T. Redel, M. Stetter, Generation of intense pulsed electron beams by the pseudospark discharge, *IEEE Trans. Plasma Sci.*, **17**, *5*, 754–757 (1989).
8. M. Hobel, J. Geerk, G. Linkev, C. Schultheiss, Deposition of superconducting YBaCuO thin films by pseudospark ablation, *Appl. Phys. Lett.*, **56**, *10*, 973–975 (1990).
9. R. Stark, J. Christiansen, K. Frank, F. Mucke, M. Stetter, Pseudospark produced electron beams for material processing, *IEEE Trans. Plasma Sci.*, **23**, *3*, 258–264 (1995).
10. R. Gilgenbach, S. D. Kovaleski, J. S. Lash, L. K. Ang, Y. T. Lau, Science and Applications of Energy Beam Ablation, *IEEE Trans. Pl. Sci.*, **27**, *1*, 150–158 (1999).
11. M. Nistor, N. B. Mandache, Electron energy distribution function of a pulsed intense electron beam, *J. Optoel. Adv. Mater.*, **7**, *3*, 1619 (2005).
12. M. Nistor, F. Gherendi, M. Magureanu, N. B. Mandache, Time-resolved spectroscopic study of pulsed electron beam ablation plasma, *J. Optoel. Adv. Mater.*, **7**, *2* (2005).
13. E. Dewald, K. Frank, D. H. H. Hoffmann, A. Tauschwitz, Plasma development in the low-pressure channel spark for pulsed intense electron beam generation, *IEEE Trans. Pl. Sci.*, **30**, *1*, 363–374 (2002).
14. Th. Witke, A. Lenk, B. Scultrich, C. Schultheiss, Investigation of plasma produced by laser and electron pulse ablation, *Surface and Coatings Technology*, **74–75**, 580–585 (1995).
15. M. Nistor, N. B. Mandache, J. Perrière, Pulsed electron beam deposition of oxides thin films, to be published in *J. Phys. D: Appl. Phys.*, 2008.